On the detection interfaces for inductive type tactile sensors

Sheng-Kai Yeh [a], Jiunn-Horng Lee [b], Weileun Fang [a,c,*]

[a] *Power Mechanical Engineering, National Tsing Hua Univ., Hsinchu, Taiwan*
[b] *National Applied Research Laboratories, National Center for High-performance Computing, Hsinchu, Taiwan*
[c] *Institute of NanoEngineering and MicroSystems, National Tsing Hua Univ., Hsinchu, Taiwan*

ARTICLE INFO

ABSTRACT

This study presents the investigation of detection interface for the inductive type tactile sensor consisted of a polymer encapsulated CMOS chip with coils and a magnetic bump. The normal tactile load will change the distance between the magnetic bump and coils, and the tactile load is then detected by the magnetic flux change of the coils. Thus, the detection interfaces include (1) the magnetic bump which acts as the contact interface, and (2) the coils (on the CMOS chip) which act as the signal pick-up interface. For the contact interface, the size and material of the magnetic bump will influence the magnetic flux of the inductive tactile sensor. The signal outputs resulted from the magnetic tactile bumps of different materials and sizes are studied. Moreover, the force responses, hysteresis measurements, and misalignment issues for magnetic bumps of different sizes are also investigated. For signal pick-up interface, two coil designs are presented to offer different sensing approaches for the inductive tactile sensor. Since the CMOS chip is implemented using the commercially available standard process (the TSMC 0.35 μm 2P4M CMOS process), multi-layer coils are achieved by using the four metal films.

© 2019 Elsevier B.V. All rights reserved.

1. Introduction

Tactile sensor plays an important role to receive touch and contact information. Presently, tactile sensors have been extensively employed in many different fields such as the robotic, industrial, and medical applications. Moreover, the touch information can be further utilized for the analog output controller (e.g. the multi-stage button for consumer products to enhance the user experience [1,2]). There are various design considerations to improve the performances of tactile sensors and further boost their applications. For instance, the tactile sensor with higher spatial resolution could imitate the human fingertips to enhance the manipulation capability of robotics [3]. In addition, the compact size tactile sensor can be embedded in handheld devices for consumer applications [2]. By using the micromachining batch fabrication processes, the MEMS (Microelectromechanical Systems) technology could fabricate and integrate compact size sensing devices. Thus, MEMS is a promising approach to extend the applications of the tactile sensor, and the MEMS tactile sensors have been extensively investigated [4–21].
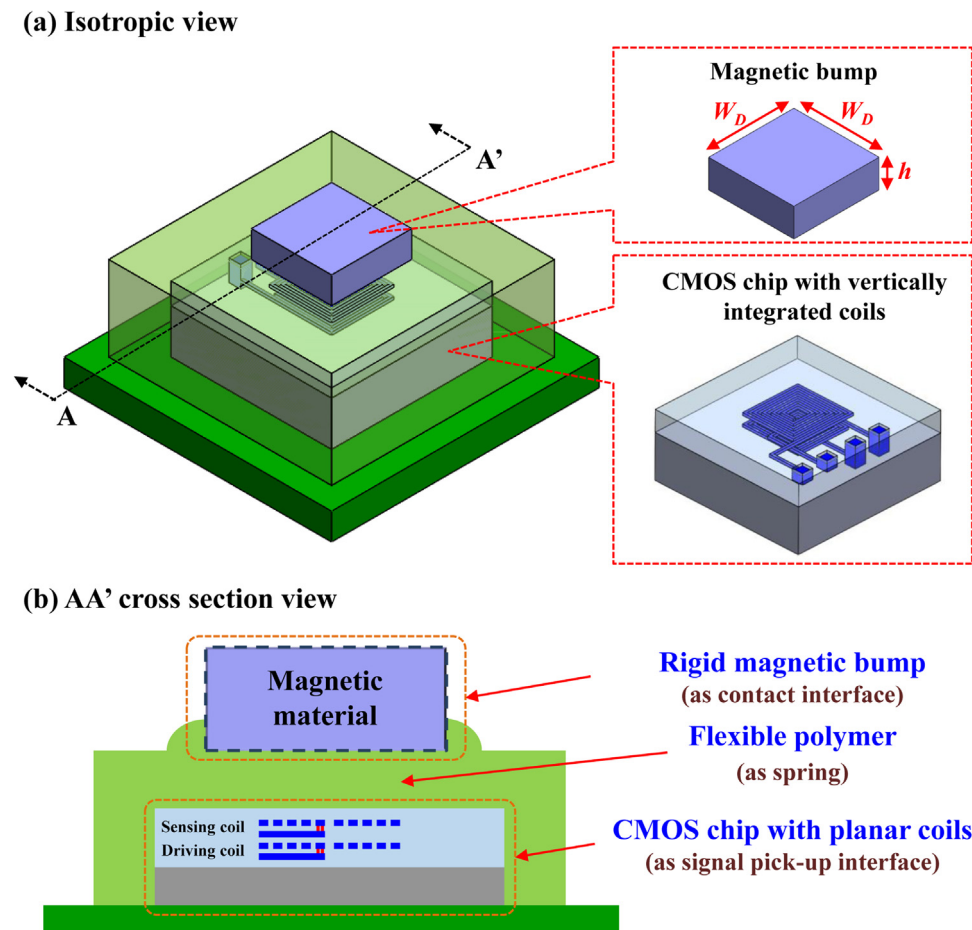
The capacitive type [4–10], and the piezo-resistive type [10–21] are the two most common sensing mechanisms for the MEMS tactile sensors. Moreover, various process technologies, such as the polymer-based process [4,11], the SOI-based process [5,6,12–16], the CMOS process [7–10,17,18], and so on, have been developed to implement the capacitive and piezo-resistive tactile sensors. In general, the capacitive type tactile sensor has higher sensitivity while the piezo-resistive type tactile sensor has larger sensing range. For capacitive and piezo-resistive type tactile sensors, the sensing signals are resulted from the deformation of flexible and suspended MEMS structures. Consequently, the initial deformations of the suspended MEMS structures due to residual stresses would be a design concern. Moreover, the suspended thin film structures are typically fragile and could be damaged by the contact tactile loads. Among the existing fabrication technologies, the CMOS process is a mature and foundry-available solution [7–10,17,18]. However, the suspended CMOS-MEMS structures usually have unwanted deformation due to the thin film residual stresses [8–10,17,18], or the CTE (coefficient of thermal expansion) mismatch of thin films [22]. The tactile sensor with inductive type sensing mechanism also attracts attention recently [23–29]. The inductive tactile sensor is consisted of the coil and the contact interface to cause and also detect the inductance variation [24–26,28,29]. Thus, the CMOS process has been adopted in [26–29] to achieve the inductive tactile sensor with no fragile suspended thin film structures.

There are several design considerations for the inductive tactile sensors reported in [26–29] despite their various advantages.

---

* Corresponding author at: Power Mechanical Engineering, National Tsing Hua Univ., Hsinchu, Taiwan.
E-mail address: fang@pme.nthu.edu.tw (W. Fang).

(a) Isotropic view

Magnetic bump

W_D W_D

h

CMOS chip with vertically integrated coils

(b) AA' cross section view

Magnetic material

Rigid magnetic bump (as contact interface)

Flexible polymer (as spring)

Sensing coil

Driving coil

CMOS chip with planar coils (as signal pick-up interface)

Fig. 1. The schematic illustrations of the proposed tactile sensor design consisted of the CMOS chip with coils, encapsulated polymer, and the magnetic bump, (a) the bird's eye view, and (b) the AA' cross-section view.
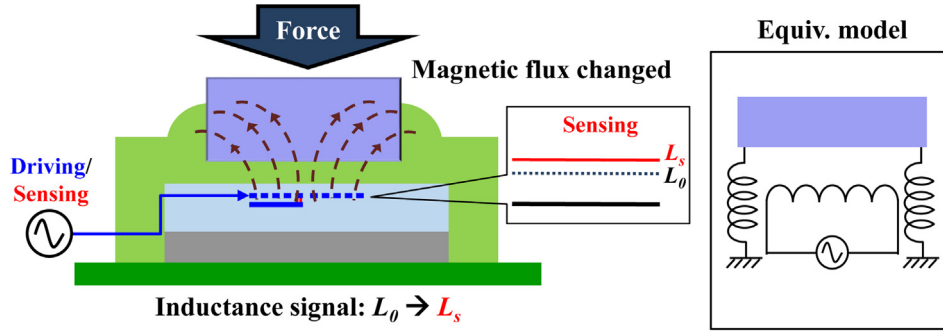
For example, the chrome steel ball contact interface in [26] could be peeled off by shear force. The distance and size of the sensing coil on the PCB could reduce the pick-up signal [27]. Thus, this study focuses on the investigation of the detection interface for the inductive type tactile sensors in [26–29]. The detection interfaces include the contact interface on the magnetic bump and the signal pick-up interface on the CMOS chip. In application, the laser-cut magnetic bumps of different sizes and materials act as the contact interfaces for tactile loads. The sensor performances such as the sensitivity, sensing range, and hysteresis, for magnetic bumps of different sizes and materials are investigated. The sensing signals influenced by the alignment of magnetic bumps with the sensing coil are also studied. Moreover, the inductive tactile sensors in [26–29] leverage the benefits of multi-layer stacking standard CMOS process (TSMC 0.35 µm 2P4M CMOS process) for the implementation of magnetic coils. Thus, the two signal pick-up interfaces of the device, the single-coil and dual-coils of the CMOS sensing chip, have been investigated. The inductance sensing using the single-coil CMOS chip and the voltage sensing using the dual-coils CMOS chip are demonstrated. By using the multiple metal layers available from the CMOS process, the driving and sensing coils are implemented and vertically integrated. As compared with the design with the sensing coil on PCB [27], the sensitivity is significantly improved.

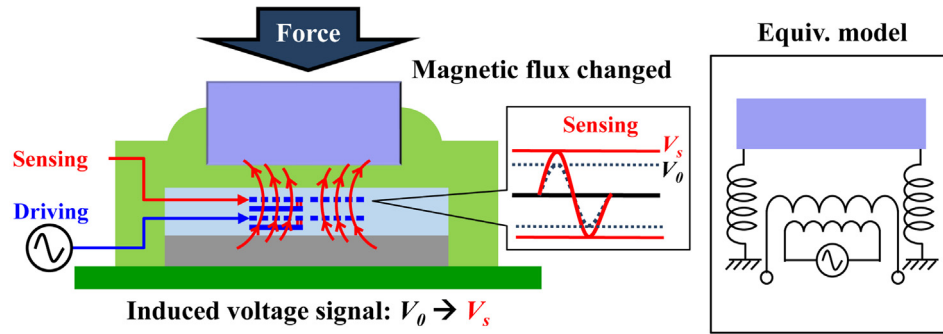## 2. Detection interfaces and the design considerations

The schematic illustration in Fig. 1a shows that the proposed inductive type tactile sensor is mainly consisted of a CMOS chip with coils. The CMOS chip is encapsulated by polymer and then

integrated with a magnetic tactile bump (square plate with dimensions $W_D \times W_D \times h$). As displayed in the zoom-in illustration, by exploiting the available metal layers in the standard foundry processes, magnetic coils of different designs can be implemented and integrated into the CMOS chip. Fig. 1b further indicates the AA' cross-section of the proposed tactile sensor. The coils on-chip are used to generate and pick-up the magnetic flux. As the tactile load is applied on the magnetic bump (contact interface of the sensor), the flexible polymer acting as the spring will be deformed. The distance between the magnetic bump and the coils will also be changed. As a result, the magnetic flux change detected by the coils is used to extract the tactile load. In summary, the characteristics of the present tactile sensor are influenced by two interfaces (named detection interfaces): (1) the contact interface on the magnetic bump, and (2) the signal pick-up interface on the CMOS chip. As depicted in Fig. 2a, the size ($W_D \times W_D \times h$ in Fig. 1a) and material of the magnetic bump will change the distribution of the magnetic flux induced by the coil. Moreover, different coil designs for the signal pick-up interface can be achieved by using the available four metal layers (metal-1 to metal-4 layers) in the CMOS process. For instance, the CMOS chip design in Fig. 2a has only a single-coil (consisted of metal-3 and metal-4 layers) for both driving and sensing. The AC signal is introduced into the coil to generate the magnetic flux. The tactile load applied on the sensing chip will cause the variation of magnetic flux and then the magnetic flux is further detected by the same coil through the inductance change (ΔL, from L_0 to L_s). The equivalent electrical-mechanical model (including magnetic bump, mechanical spring, and the sensing coil with AC input) is also illustrated. In addition, the CMOS chip design in Fig. 2b is

(a) Sensing mechanism (single-coil signal pick-up)

(b) Sensing mechanism (dual-coils signal pick-up)

Fig. 2. The sensing mechanisms of the proposed inductive type tactile sensor using different signal pick-up (cross-section of AA' in Fig. 1), the displacement of the magnetic bump caused by the tactile force will lead the magnetic flux change on sensing coil, and then (a) detected by the inductance signal change on the single-coil sensing design, and (b) detected by the voltage signal change on the dual-coils sensing design.

equipped with a driving coil (consisted of metal-1 and metal-2 layers) and a sensing coil (consisted of metal-3 and metal-4 layers). According to the mutual inductance between these two coils, the variation of magnetic flux (from driving coil) due to the tactile load is detected by the voltage change of sensing coil (ΔV, from V_0 to V_s). The equivalent electrical-mechanical model is also presented. To improve the performances of inductive sensors [26,27], the influence of detection interfaces including the tactile bump and coils are investigated.
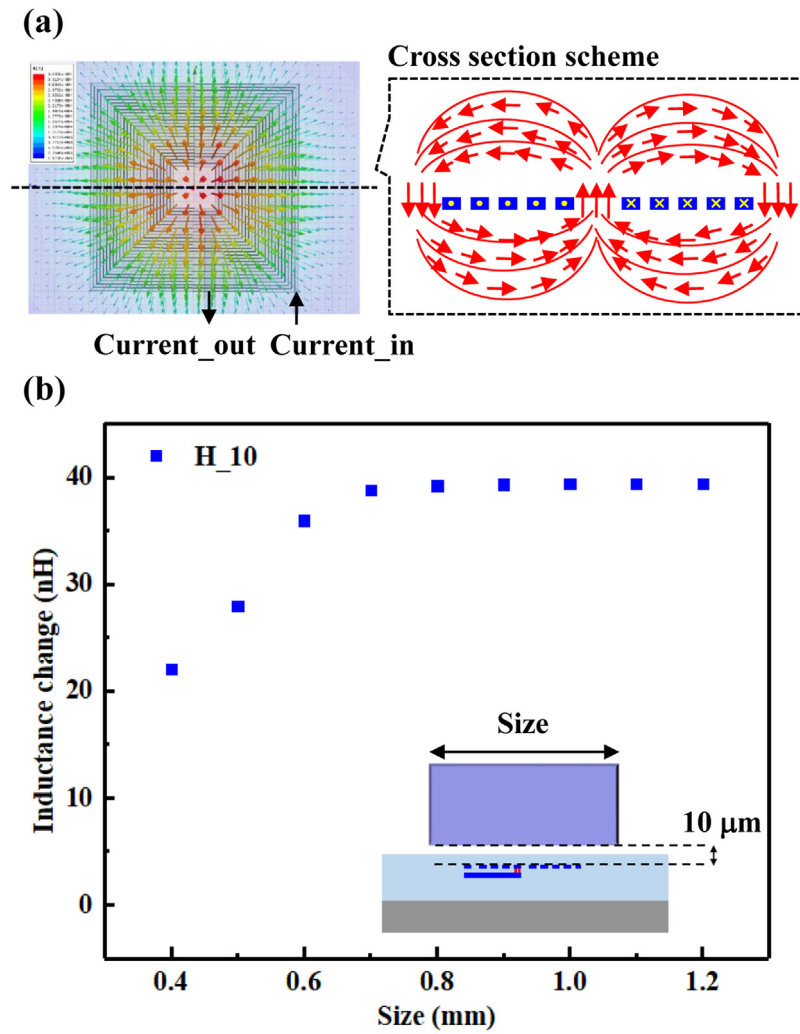
The commercial finite element method (FEM) softwares (including ANSYS and Ansoft Maxwell) are utilized to predict sensor performances and characteristics. The polymer deformation of the tactile sensor resulted from the tactile load is predicted by ANSYS first, and then the magnetic flux change of planar coil is simulated by Ansoft Maxwell. To meet the requirement of minimum spatial resolution of the human finger for micro tactile sensor applications [3], the in-plane dimensions of the sensing coil are designed to be 0.6×0.6 mm^2. The size effect of the square magnetic bump is then investigated. Fig. 3a presents the simulation results and the cross-section scheme of the magnetic flux distribution of the planar sensing coil after the input of current. Simulation results in Fig. 3b show the inductance change of coil ΔL_0 (no tactile load is applied) before and after adding the square magnetic bump of different sizes (0.4×0.4 mm^2 to -1.2×1.2 mm^2 with 300 μm thickness) on top of the coil. Note that the gap between the coil and the magnetic bump was roughly selected as 10 μm (by considering the thickness of the passivation layer and the flatness of magnetic bump and the CMOS chip). Moreover, the magnetic bumps smaller than 0.4×0.4 mm^2 are not investigated in simulations since they are difficult to handle during the fabrication processes. Simulation results indicate the inductance change of coil ΔL_0 is increased with the size of the magnetic bump. As limited by the area of magnetic flux from the coil (as

shown in Fig. 3a), the ΔL_0 has no significant change when the size of the magnetic bump exceeds 0.8×0.8 mm^2. In short, the magnetic bumps investigated in this study are ranging from 0.4×0.4 mm^2 to 0.8×0.8 mm^2.
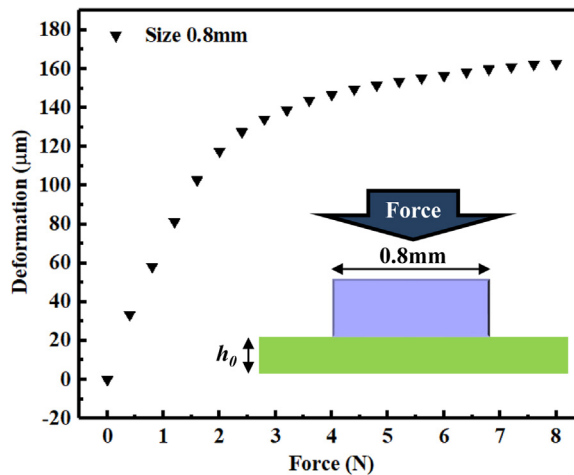
In this study, the nonlinear Mooney-Rivlin model is employed in FEM to evaluate the large deformation of polymer [30–32]. To simplify the numerical analysis of the proposed device, the Mooney-Rivlin model with two parameters is used [32],

$$W = C_{10}(I_1 - 3) + C_{01}(I_2 - 3) \tag{1}$$

where W is the strain energy density, C_{10}, C_{01} are Mooney-Rivlin constants, and I_1, I_2 are the first and second strain invariants, respectively. A 210 μm thick polymer with a rigid square bump of 0.8×0.8 mm^2 is prepared as the test sample to extract the Mooney-Rivlin constants in Eq. (1). Measurements in Fig. 4 show the polymer deformations of the test sample after loads applied on the bump. By curve fitting of the results in Fig. 4, the Mooney-Rivlin constants are extracted as $C_{10} = 0.1$ MPa and $C_{01} = 0.0625$ MPa. After that, the polymer deformations of sensors with different bump sizes are predicted by the FEM. Fig. 5 shows the simulation results of the sensors with five bump sizes (0.4×0.4 mm^2, 0.5×0.5 mm^2, 0.6×0.6 mm^2, 0.7×0.7 mm^2, and 0.8×0.8 mm^2). Firstly, simulations in Fig. 5a present the variation of polymer deformations with tactile loads. For a given tactile force, the smaller bump will introduce a higher pressure load and a larger deformation on the polymer. Moreover, the saturation of the forces is also observed in the simulation of different bump sizes. Secondly, simulations in Fig. 5b further depicts the variation of inductance change ΔL with the gap (10 μm~210 μm) between the bump and coils. Similar to the prediction in Fig. 3, the bump with larger planar dimension could receive more magnetic flux and hence has higher inductance. By combining the simulation results in Fig. 5a and b, the variation of inductance change ΔL with
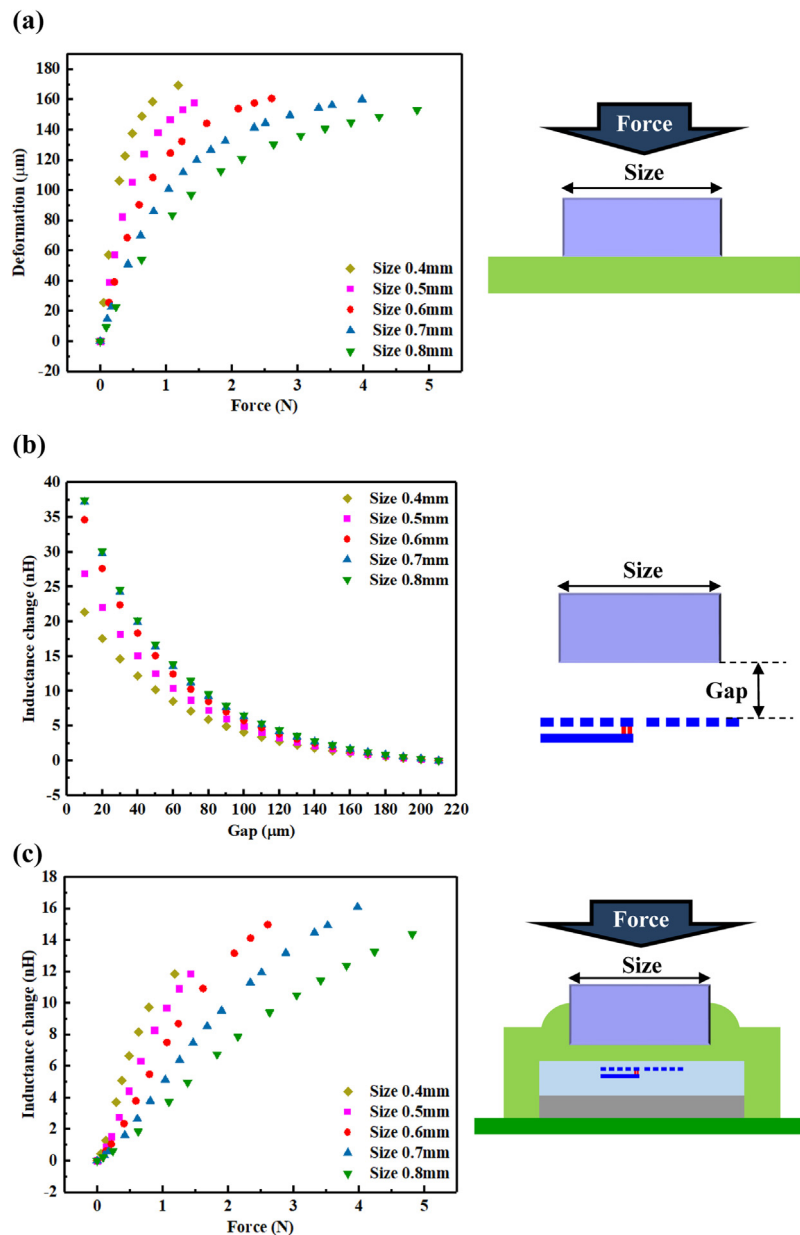
Fig. 3. Simulation results of signal variation for the different sizes of the magnetic bump: (a) the simulated magnetic flux distribution of the planar sensing coil, and (b) the inductance change of coil ΔL_0 before and after adding the square magnetic bump of different sizes on top of the coil.

Fig. 4. Load-deformation tests on polymer specimen to extract the polymer material constants for FEM model.

tactile load is further determined in Fig. 5c. In summary, according to the linear fit (99%) of simulation results in Fig. 5c, as the tactile bump size is increased from 0.4×0.4 mm^2 to 0.8×0.8 mm^2, the sensing range is increased from $0\tilde{0}.6$ N to $0\tilde{3}.8$ N, whereas the sensitivity is decreased from 13.6 nH/N to 3.4 nH/N.

Finally, the dual-coils (sensing and driving coils) design is also investigated in this study. The coupling coefficient between the driving and sensing coils would affect the voltage output of the sensing coil. For dual-coils design, this study fabricates and further vertically integrates the driving and sensing coils using the CMOS

Fig. 5. Simulation results: (a) the polymer deformation when tactile loads are applied on the magnetic bump of different sizes, (b) the variation of inductance change with the gap between the magnetic bumps and the sensing coil, and (c) the inductance change when tactile loads are applied on the magnetic bump of different sizes.

process. Thus, both of the driving and sensing coils have the planar dimensions of 0.6×0.6 mm^2, and the distance between the sensing and driving coils is 1 μm. As compared with the design in [27], the sensing coil on the chip is 0.5×0.5 mm^2, however, the driving coil on PCB (printed circuit board) is 16×16 mm^2. Moreover, the distance between the driving and sensing coils is 1.6 mm. According to the simulation from Ansoft Maxwell, the coupling coefficient of the proposed dual-coils design is near 0.94, which is 1 order higher than that of [27].

3. Fabrication and results

The fabrication processes of the proposed device are presented in Fig. 6. The proposed tactile sensing chip with vertically integrated coils was implemented by the TSMC 0.35 μm 2P4M standard CMOS process and the in-house post-CMOS processes. Firstly, the stacking of the dielectric layers and metal layers were fabricated by using the standard TSMC processes, as illustrated in Fig. 6a. Note the

bond pads of the coils were exposed for electrical connection. After that, as depicted in Fig. 6b, the CMOS chip was then wire-bonded on PCB and the wires were protected by epoxy to prevent damage. As shown in Fig. 6c, the CMOS chip was then encapsulated by the polymer (Dow Corning® SYLGARD PDMS 184) using the molding process. The initial gap h_0 between the magnetic bump and CMOS chip defined in this process was 206 ± 14 μm. As presented in Fig. 6d, the magnetic bumps are fabricated by the laser cut from commercially available metal sheets. After the curing of encapsulated polymer on the CMOS chip, the magnetic bump was fixed to the polymer-encapsulated sensing chip by using the polymer adhesive. Note that the fabrication processes were simple, and no fragile suspended thin film structures were required for the present device.

The micrographs in Fig. 7a present the CMOS chips in the pack and the zoom-in of the CMOS chip with coils. The planar dimension of the driving coil (metal-1 and metal-2) is designed to be identical with that of the sensing coil (metal-3 and metal-4) to increase
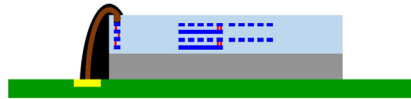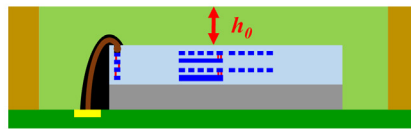
A-A' cross-section view
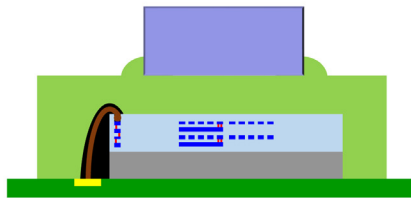
(a) Chip prepared by TSMC

(b) Wire bonding and wire protection

(c) CMOS chip polymer molding and curing

h_0

(d) Bump integration and demolding

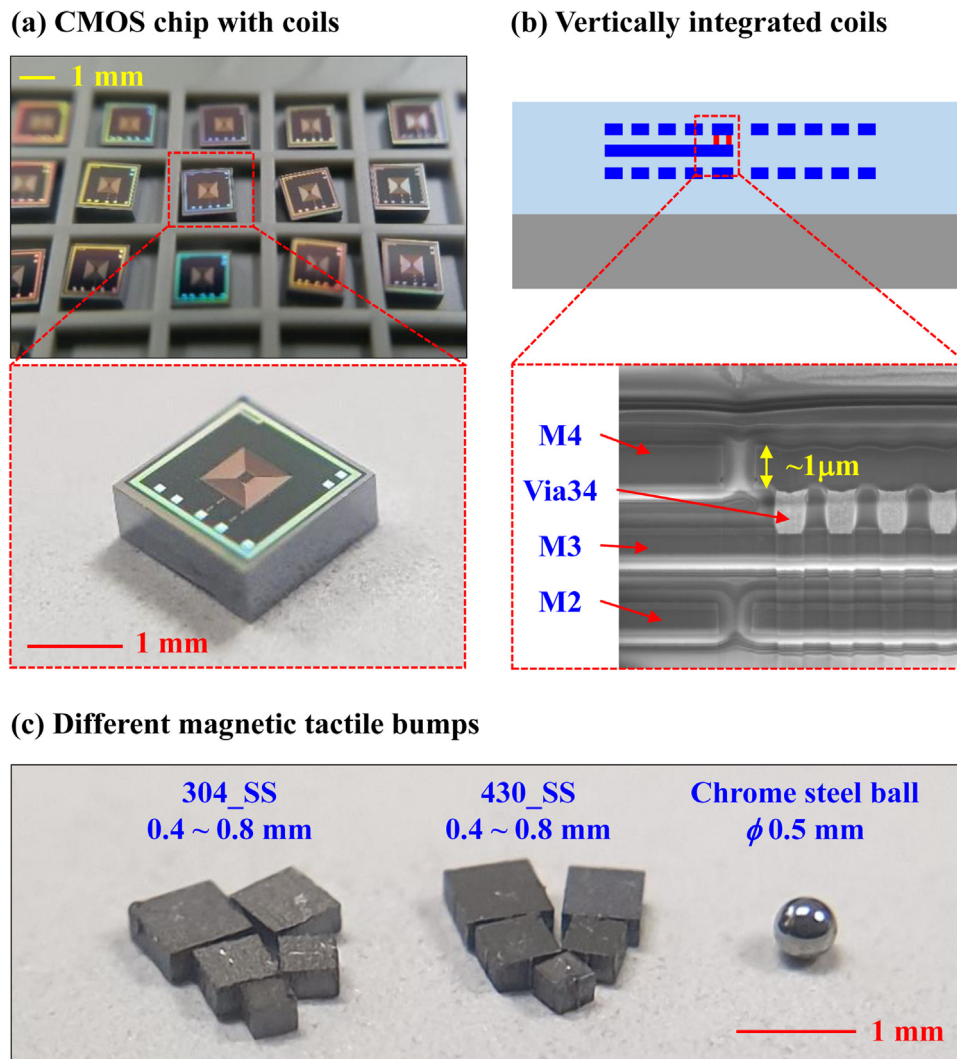Oxide Metal Via Mold Silicon Polymer Epoxy Bump PCB

Fig. 6. Fabrication processes of the device, (a) the CMOS chip with sensing coils fabricated by the TSMC foundry using the standard process, (b) wire-bonding for electrical connection, (c) CMOS chip polymer encapsulation and curing, and (d) pick-place and then fix, by adhesive polymer, the laser-cut magnetic bump to complete the device.

the coupling coefficient. Thus, the coils have planar dimensions of $0.6 \times 0.6 \, mm^2$, and each coil has a total number of 25 turns. By using the CMOS technology, the coils can be precisely defined, vertically integrated, and aligned. The cross-section micrograph prepared by the FIB (focus ion beam) in Fig. 7b shows the multi-layer stacking of 2P4M CMOS chip. The metal-3 and metal-4 layers, and the tungsten via to connect these two layers are observed. These layers form the sensing coil. The metal-2 layer for the driving coil is also observed (note the metal-1 layer is not shown in this cross-section). Note all of the metal layers are protected by the dielectric films through the CMOS process. The micrographs in Fig. 7c, respectively, display various magnetic bumps with distinct materials and sizes. In short, the materials adopted as the sensing interface including the 304 and 430 stainless steel (abbreviated as SS) bumps and the chrome steel ball (used in [26,27,29]). The commercially available chrome steel ball has a diameter of 0.5 mm. The planar dimensions of magnetic bumps prepared by laser-cut are $0.4 \times 0.4 \, mm^2$, $0.5 \times 0.5 \, mm^2$, $0.6 \times 0.6 \, mm^2$, $0.7 \times 0.7 \, mm^2$, and $0.8 \times 0.8 \, mm^2$. Note the accuracy of the laser cut process is $\pm 5 \, \mu m$. The thicknesses of 304 and 430 stainless steel bumps are $300 \, \mu m$ (with the accuracy of $\pm 3 \, \mu m$). Micrographs in Fig. 8 show the integration of the CMOS sensing chip with bumps (430 stainless steel, denoted as SS_dimension in the figure) of different sizes. The CMOS sensing chip under the bump is wire bonded to the PCB to form the device under test (DUT).

4. Results and discussions

This study has performed the experiments to evaluate the influence of the detection interface (including the magnetic bump and sensing coils) on the inductive tactile sensor. Firstly, the inductance changes resulted from different sizes and materials of magnetic bumps are characterized. After that, various experiments to evaluate the sensor performances (i.e. the sensing signals versus tactile loads, hysteresis, and alignment issue) for devices of different contact interfaces (i.e. the sizes and materials of magnetic bumps) are performed. Finally, the influence of the dual-coils pick-up interface (i.e. the vertically integrated magnetic coils on the CMOS chip) is characterized. Table 1 summarizes the specifications and comparisons of the proposed CMOS inductive type tactile sensors using different detection interfaces.

This study has established the tests in Fig. 9a to evaluate the influence of the size and material of the magnetic bump. The inductance signals of the sample without magnetic bump (CMOS chip with a planar coil, the top one in Fig. 9a) were measured first. After that, the magnetic bumps of different sizes and materials were placed on the CMOS chip (the bottom one in Fig. 9a), and the inductance signals of these samples were also measured. Measurements in Fig. 9b show the inductance change after placing the magnetic bump on the CMOS sensing chip. The error bar for each data point (the magnetic bump with a specific size and material) is

(a) CMOS chip with coils

(b) Vertically integrated coils
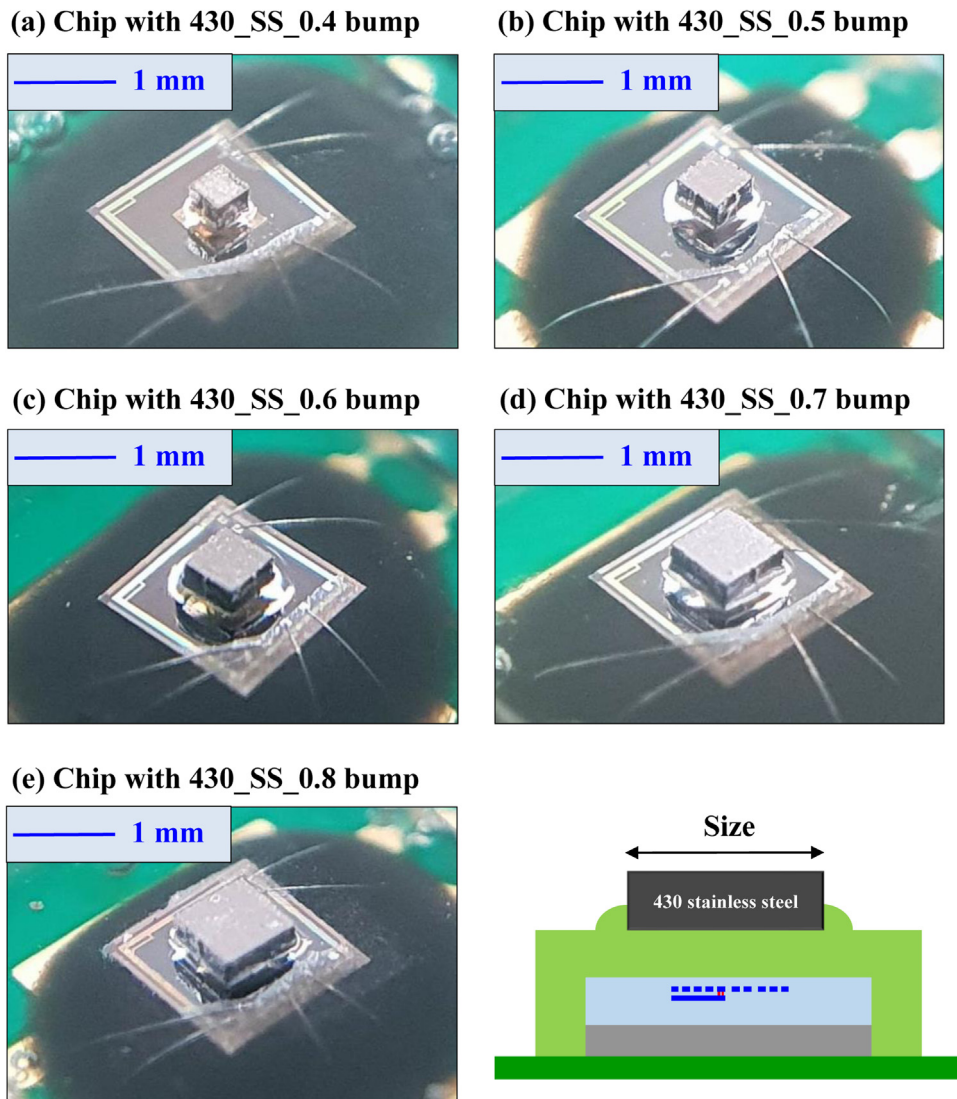

(c) Different magnetic tactile bumps

Fig. 7. Typical fabrication results of the chip and the magnetic bumps, (a) the CMOS sensing chip fabricated by the TSMC foundry, (b) the cross-section micrograph (prepared by FIB) of the CMOS chip with the stacking of multi-layers, and (c) magnetic tactile bumps with different materials and sizes.

from the measurements of at least ten samples. The results depict the difference of inductance change resulted from magnetic bumps of different sizes and materials. Magnetic bumps of two different materials, the 430 stainless steel and the 304 stainless steel, are characterized. The planar dimensions of magnetic bumps are ranging from 0.4×0.4 mm^2 to 0.8×0.8 mm^2, as mentioned in Section 2. In comparison, the inductance change introduced by the 0.5 mm diameter chrome steel ball used in [26,27] is also measured. The results indicate the inductance signals have no significant change for the 304 stainless steel bump, which may be due to the low permeability of 304 stainless steel. In comparison, the relatively permeability of 430 stainless steel is 2~3 order higher than that of the 304 stainless steel [33–35]. Thus, the 304 stainless steel is not appropriate for the application of the inductive tactile sensor. Therefore, the following tests are focused on the 430 stainless steel bump. Significant inductance changes are achieved for the 430 stainless steel bump with the size larger than 0.5×0.5 mm^2. Moreover, the inductance change is increasing with the dimension of magnetic bump and then reaches a saturation value when the size of the bump size larger than that of the coil (0.6×0.6 mm^2). Measurements agree with the trend predicted in Fig. 3b. Note that the magnetic bump with the size of 0.4×0.4 mm^2 has poor signal

output compared with others, which may be due to the magnetic properties variations resulted from laser cutting [36] (The coercivity of SS_0.4 is one order higher than others after the verification using VSM).

4.1. Sensor performances for the magnetic bump of different sizes

The testing system in Fig. 10 is established to characterize the performances of the proposed tactile sensors. The DUT shown in Fig. 8 is fixed on the tri-axial motor stage, and hence the in-plane (x and y axes) alignment and the out-of-plane (z-axis) displacement of the DUT are controlled by the motor stage through the controller. The sensor is under a tactile load through the probe of a commercial force gauge when the DUT has a prescribed z-axis displacement specified by the positioning stage. Meanwhile, the tactile load applied on the sensor is monitored by the commercial force gauge (FSH-50 N, YOTEC Precision Instrument, Taiwan, 0.01 N resolution with a maximum loading of 50 N). The commercial LCR meter (Agilent, 4980A) applies an AC signal to the coil of the CMOS sensing chip and also detects the inductance of the coil. Thus, the inductance changes varying with tactile loads can be measured.

(a) Chip with 430_SS_0.4 bump

(b) Chip with 430_SS_0.5 bump

(c) Chip with 430_SS_0.6 bump

(d) Chip with 430_SS_0.7 bump

(e) Chip with 430_SS_0.8 bump

Fig. 8. Typical fabrication results of the devices, (a–e) the CMOS chips are, respectively, integrated with the 430 stainless steel magnetic bump of different sizes (0.4×0.4 mm^2 – 0.8×0.8 mm^2 with 300 μm thickness). The CMOS chips are also wire bonded on the PCB for the following performance tests.

Measurement results in Fig. 11 show the force responses of the inductive tactile sensors with magnetic bumps of different sizes. The material of the magnetic bump is 430 stainless steel and the size of the bump is ranging from 0.4×0.4 mm^2 to 0.8×0.8 mm^2. Fig. 11a summarizes the force responses of all samples and Fig. 11b–f further, respectively, show the force responses of samples with different sizes. As shown in Fig. 11a, b, the inductance changes of the 0.4×0.4 mm^2 magnetic bump is very small which has been expected from the tests in Fig. 9. Thus, despite the 0.4×0.4 mm^2 magnetic bump having a larger polymer deformation, it is unable to cause a decent sensing signal (inductance change). Moreover, the relations of inductance change and tactile force in Fig. 11c–f exhibit the characteristics of piecewise-linearity. The hardening effect of the polymer under compression [31] is the reason to cause the drop of sensing signal at higher loads. As indicated in the figures, this study depicts the two different sensitivities (S_1 and S_2) for the presented sensors based on the slope of piecewise-linear curve fitting, and the sensing range of the presented sensors are determined by the turning points. The results show that as the magnetic bump increases from 0.5×0.5 mm^2 to 0.8×0.8 mm^2 the sensing range extends from 1.4 N to 3.7 N, however, the sensitivity drops from

20 nH/N to 9.7 nH/N. The sensing ranges predicted in Fig. 5c agree well with the measurements. However, the measured sensitivities are 2.1-fold to 2.85-fold higher than the simulations in Fig. 5c. The difference could be due to the variation of material properties (e.g. magnetic properties of the magnetic bump) in simulation models.
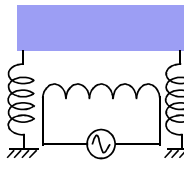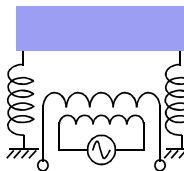
The polymer extensively employed in the tactile sensor as the protection and buffer layer or force transmission layer [4,11,13–16,18] has the concern about the stress-strain hysteresis [30]. This study further investigates the hysteresis phenomena for magnetic bumps of different sizes. The loading and un-loading tests are performed by using the experiment setup in Fig. 10 to characterize the hysteresis phenomena. Measurement result in Fig. 12a presents the load-deflection curve on the pure polymer to show its hysteresis characteristic. The loading-unloading curves measured in Fig. 12b–f, respectively, depict the hysteresis effects of the tactile sensors with magnetic bumps of different sizes. The results indicate a larger magnetic bump will increase the hysteresis. This is a design concern for applications.

In this study, the magnetic bump is picked by the vacuum pen and then placed on the CMOS sensing chip by using the positioning
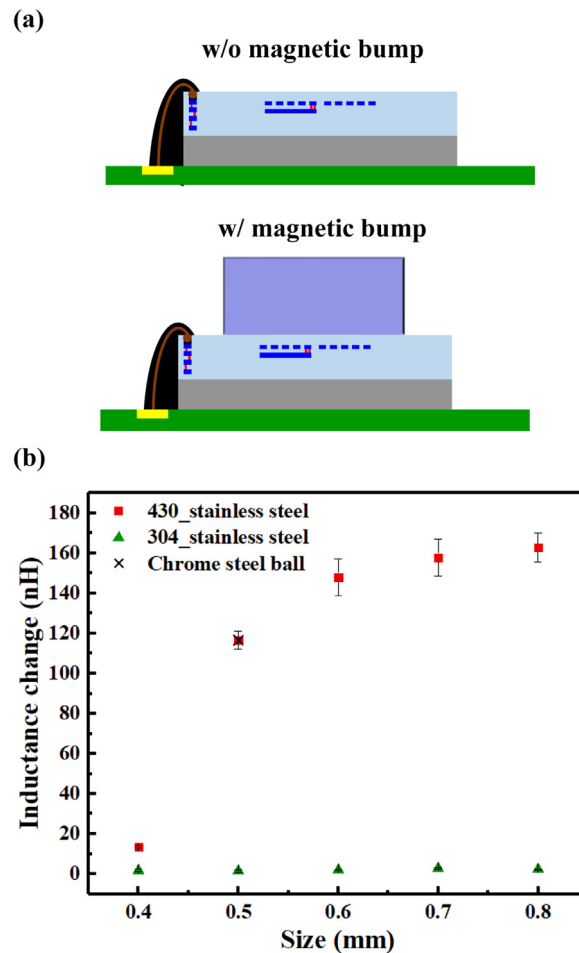
Table 1
The specifications and performances of the presented CMOS inductive tactile sensors with different detection interfaces, (a) devices with single-coil signal pick-up, and (b) device with dual-coils signal pick-up.

a. Single-coil signal pick-up	Specifications and performances of the sensors					Unit
	Size of sensing coil			0.6 × 0.6		mm²
	Size of chip			1.7 × 1.7		mm²
	Polymer thickness			206±14		μm
	Tactile bump size (430 stainless steel)	0.4 × 0.4	0.5 × 0.5	0.6 × 0.6	0.7 × 0.7	0.8 × 0.8	mm²
	Sensing range	0-0.9	0-1.4	0-2	0-2.9	0-3.7	N
	Sensitivity (only S_I)	4.4*	20	19.5	14	9.7	nH/N

b. Dual-coils signal pick-up	Specifications and performances of the sensors			Unit
	Size of sensing coil		0.6 × 0.6	mm²
	Size of chip		1.7 × 1.7	mm²
	Polymer thickness		206±14	μm
	Tactile bump size (430 stainless steel)		0.6 × 0.6	mm²
	$V_{driving}$ in V_{pp}, @ 30MHz	1	3	5	V
	Sensitivity (only S_I)	1.05	3.30	4.89	mV/N

[a]Poor signal output due to the fluctuation of material properties after the laser-cut process.

Fig. 9. (a) The test scheme, and (b) measurement results, to evaluate the inductance change of the sensing coil before and after adding the magnetic bump on the sensing chip. The magnetic bump of different magnetic materials and sizes are characterized.
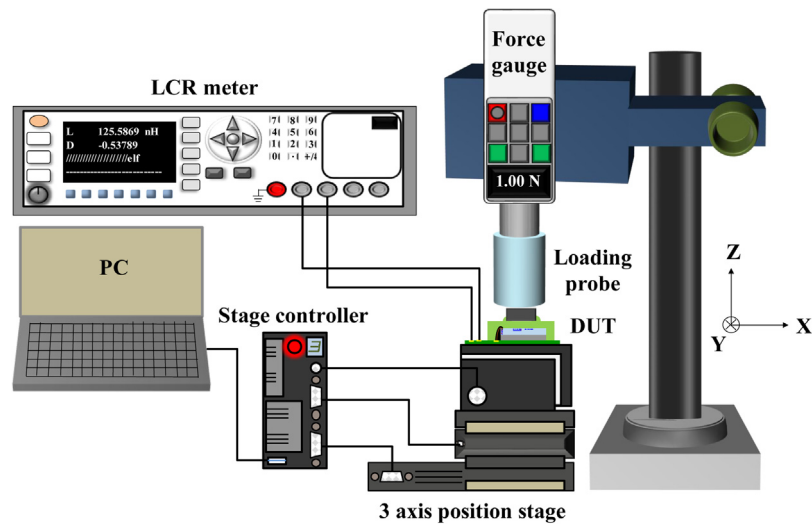
Fig. 10. The test setup to measure the variation of inductance signals with tactile loads.

stage. Thus, the testing setup in Fig. 13a is established to investigate the signal variation due to the misalignment of the magnetic bump and sensing coil. The illustration and micrograph show the frame with alignment ruler marks (the length between two marks is 100 μm) fabricated by laser cutting. During the tests, the coil is placed at the center of the alignment frame, as depicted in the left-hand side illustration in Fig. 13a. The space with 600 μm in length is also marked at the center of each side on frame to align the frame and coil (as indicated by red dash lines in figure). Thus, the misalignment of magnetic bump with the coil can be expressed by its center offset (|x|, |y|), as depicted in the right-hand side micrograph. As shown in the micrographs in Fig. 13b, magnetic bumps of two different sizes (0.5×0.5 mm^2 and 0.8×0.8 mm^2 are, respectively, smaller and larger than the sensing coil) with different alignment conditions are prepared for the tests. Measurement results in Fig. 13c, show that the sensitivities of tactile sensors (including S_1 and S_2) have a less than ±15% offset when the center misalignment of magnetic bumps (for both 0.5×0.5 mm^2 and 0.8×0.8 mm^2) is smaller than 100 μm for both axes. In addition, the sensitivities of tactile sensors (including S_1 and S_2) have a 50~60% offset when the center misalignment of magnetic bumps (for both 0.5×0.5 mm^2 and 0.8×0.8 mm^2) is 300 μm for both axes. Note that the commercially available pick-place facilities have the alignment accuracy of ranging from ±2.5 μm to ±50 μm.
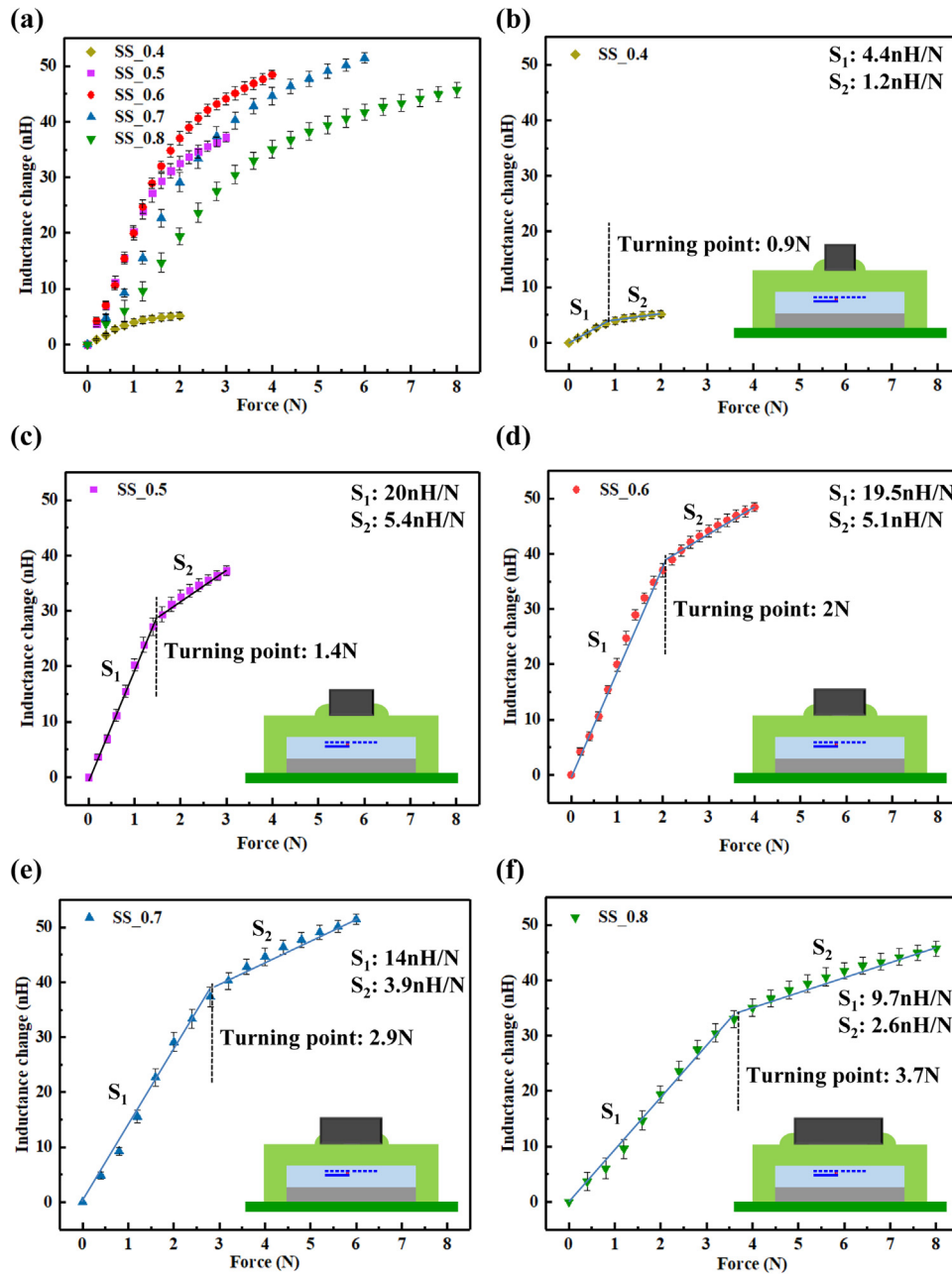
4.2. Signal pick-up (voltage output) using dual-coils design

Finally, the CMOS chip with single-coil and dual-coils signal pick-up designs shown in Fig. 2 are characterized. This study employs the CMOS chip with 0.6×0.6 mm^2 stainless steel magnetic bump (SS_0.6) as the test sample. This study establishes the test setup to evaluate the performance of the dual-coils design in Fig. 2b. As shown in Fig. 14a, the AC signal $V_{driving}$ from the function generator (Agilent 33220A) is applied on the driving coil, and the voltage $V_{sensing}$ output from the sensing coil is monitored by the oscilloscope (Tektronix DPO 3014). After specifying the tactile load on the magnetic bump using the force gauge, the variation of $V_{sensing}$ from the sensing coil is measured. Note that the $V_{sensing}$ from the sensing coil is sensitive to the frequency of $V_{driving}$ of the driving coil. The dual-coils system in this study has a resonant frequency of 38.4 MHz and a flat frequency response region of 28~34 MHz. Thus, to avoid the variation of the sensing signal induced by the fluctuation of the driving frequency, 30 MHz (which is within
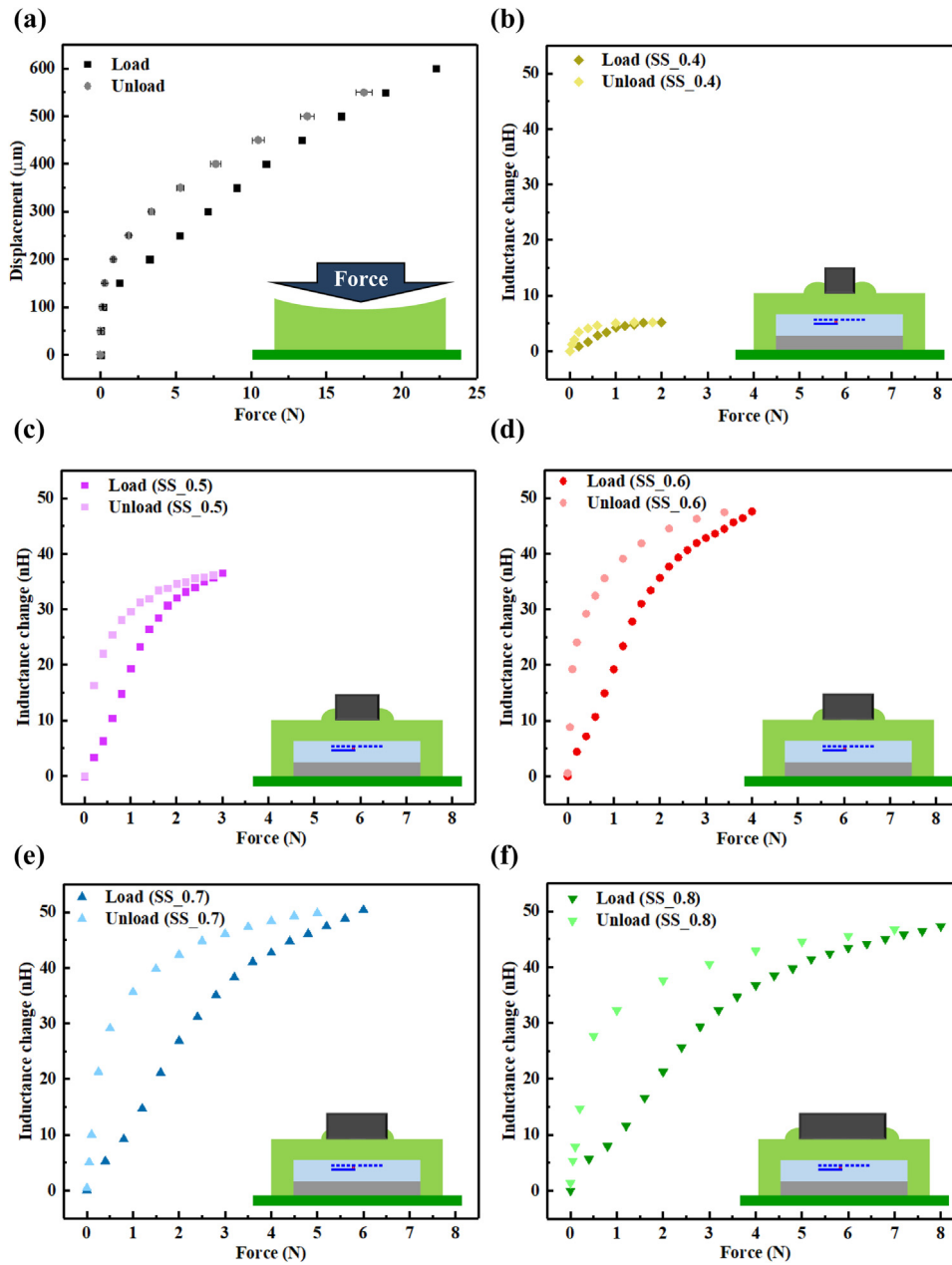
the flat frequency response region) is selected for the following electrical test and tactile force response measurements. Fig. 14b presents the initial output voltages $V_{sensing}$ from the sensing coil when different $V_{driving}$ are applied to the driving coil. Measurements in Fig. 14c further depict the variation of $V_{sensing}$ with tactile loads at three different $V_{driving}$ (15 V_{pp}). Note the $V_{sensing}$ of dual-coils design could receive a gain factor by increasing the $V_{driving}$. As compared with the results in [27], the vertically integrated dual-coils sensing design could increase the sensitivity to near 1 order. Fig. 14d further summarizes the inductance output (in Fig. 11d) from the single-coil design (in Fig. 2a) and the voltage output (5V_{pp} driving voltage case in Fig. 14c) from the dual-coils design (in Fig. 2b). Since both of these two sensing approaches are based on the variation of magnetic flux, the sensing signals (for both inductance and voltage changes) varying with tactile loads exhibit the same trend. In summary, the CMOS-based sensing chip could offer two methods for the signal pick-up of the inductive tactile sensor.

5. Conclusions

This work presents the investigations of detection interfaces for the inductive type tactile sensor consisted of a polymer-encapsulated CMOS chip with coils and a magnetic bump. The chip is fabricated by the TSMC 0.35 μm 2P4M CMOS process and the in-house polymer molding. Since the polymer is employed to act as the spring, no fragile suspended thin film structures are required for such inductive tactile sensor. The deformations introduced by the CTE mismatch and residual stresses of thin films are prevented. The detection interface of the proposed tactile sensor is composed of the signal pick-up interface (the coils on the CMOS chip) and the contact interface (the magnetic bump). For the signal pick-up interface, the vertical integrated coils are implemented using the multi-layer CMOS process. Thus the inductance detection using the single-coil sensing design and the voltage detection using the dual-coils sensing design are demonstrated. For the contact interface, the magnetic bumps of different sizes and materials are prepared by the laser-cut process. The sensor performances such as the sensitivity, sensing range, and hysteresis for magnetic bumps of different sizes and materials are investigated. Measurements indicate the 304 stainless steel is not suitable for the magnetic bump, and the 430 stainless steel shows considerable signal output (as bump sizes larger than 0.5×0.5 mm^2). Moreover, for the 430 stainless steel
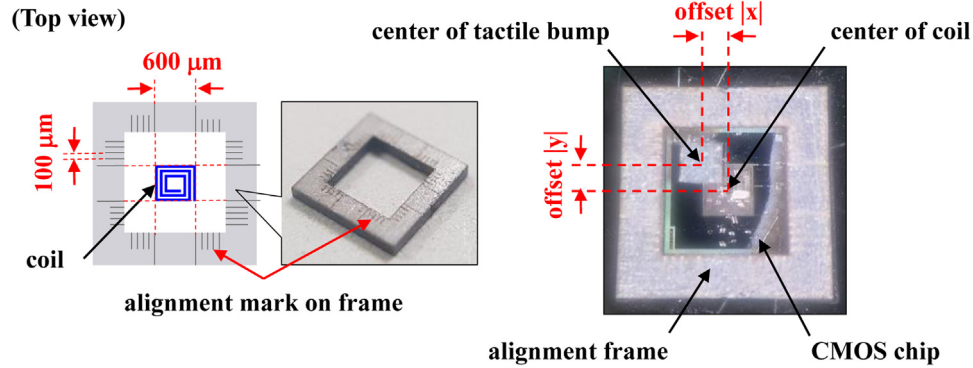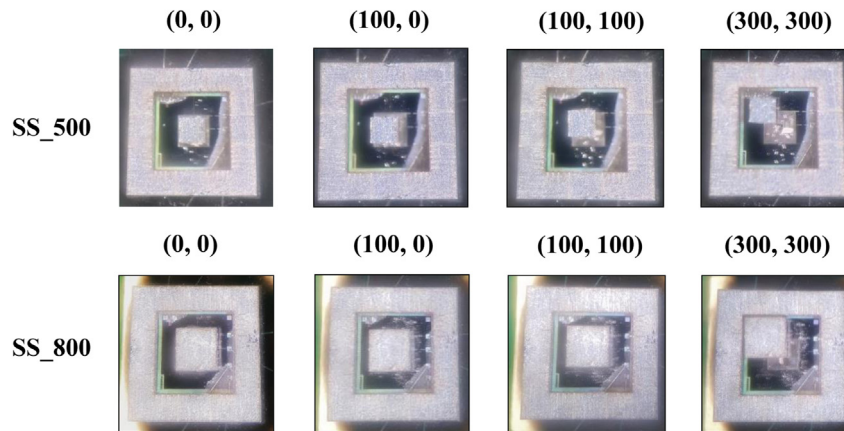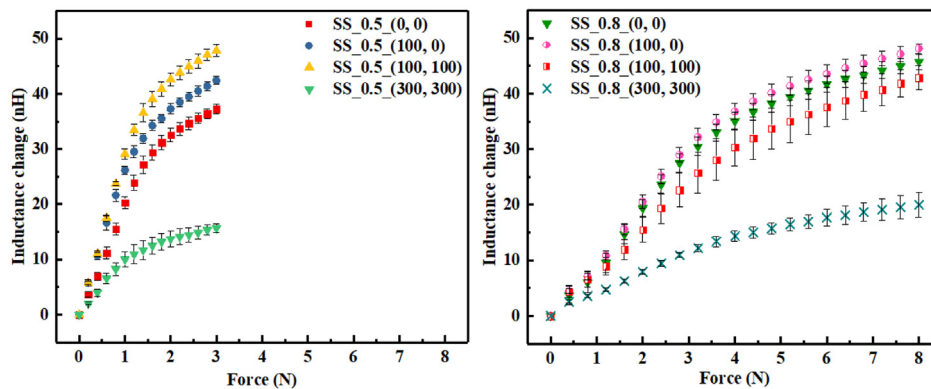
Fig. 11. Force responses of devices with the 430 stainless steel magnetic bump of different sizes (signal pick-up using the single-coil sensing design), (a) comparison of force responses for different samples, and (b–f) force responses, respectively, for sensors with the magnetic bump of different sizes.

Fig. 12. Hysteresis measurements of devices with the 430 stainless steel magnetic bump of different sizes (signal pick-up using the single-coil sensing design), (a) hysteresis for loadings on pure polymer, and (b–f) hysteresis for loadings on sensing chips with different magnetic bumps (SS_0.4, SS_0.5, SS_0.6, SS_0.7, and SS_0.8).
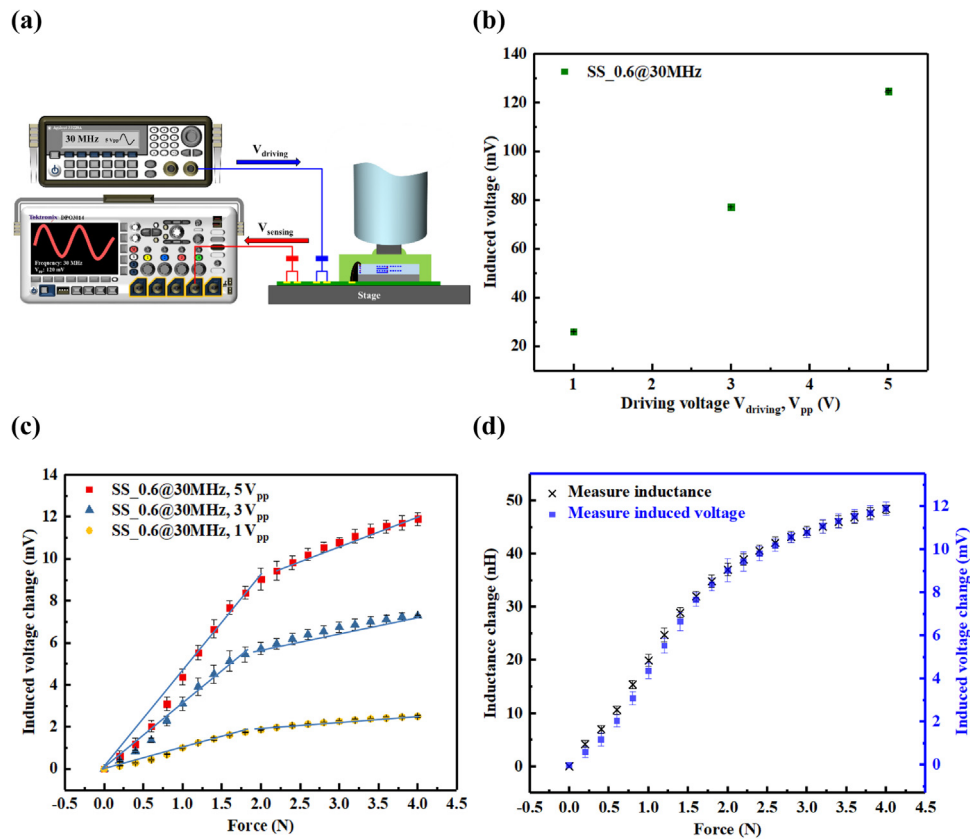
Fig. 13. Measurements to evaluate the influence of the misalignment of the tactile bumps (SS_500 and SS_800), (a) the test setup to specify the misalignment, (b) micrographs of misalignment conditions, and (c) measurement results for different misalignment conditions.

magnetic bumps, the sample with larger magnetic bump has higher sensing range, more severe hysteresis, and lower sensitivity. Note that the very poor sensitivity of $0.4 \times 0.4\,mm^2$ magnetic bump may be due to the change of magnetic properties caused by the temperature elevation from laser-cut process. It is worth to investigate the influence of laser-cut process on the change of material properties. Finally, the sensitivities of tactile sensors have a less than ±15% offset when the center misalignment of the magnetic bumps (for both $0.5 \times 0.5\,mm^2$ and $0.8 \times 0.8\,mm^2$) is smaller than 100 μm for both axes. Table 1 summarizes the specifications of the proposed CMOS inductive type tactile sensor with different detection interfaces. Note that the plate magnetic bump in this study is attached to the polymer using PDMS adhesive. Measurements indicate the shear force to peel off the magnetic bump is near 0.06 N. In compar-

ison, the shear force to peel off the ball magnetic bump in [26,27] is 0.05 N. Thus, a better adhesive is required to enhance the bonding strength of contact interface. The encapsulation of the magnetic bump with polymer as presented in [28] is another approach to avoid the peel off of the contact interface by shear load. Moreover, the durability of the polymer material (PDMS) is also an important concern for future applications.

Fig. 14. Voltage output measurements using the sensing chip with the dual-coils design, (a) the test setup for force response and driving and sensing signals, (b) variation of initial induced voltage on the sensing coil with the voltage applied on the driving coil, (c) force responses of dual-coils sensing design with different driving voltages, and (d) comparison of force responses, respectively, measured from the single-coil sensing design (inductance signal output) and the dual-coils sensing design (voltage signal output).

References

[1] Force Sensing Solutions, NextInput Inc., San Francisco, U.S, 2012.
[2] Iphone6s, Apple Inc., California, U.S, 2015.
[3] R.S. Dahiya, M. Valle, Robotic Tactile Sensing: Technologies and System, Springer Science & Business Media, 2012.
[4] M.-Y. Cheng, X.-H. Huang, C.-W. Ma, Y.-J. Yang, A flexible capacitive tactile sensing array with floating electrodes, J. Micromechanics Microengineering 19 (2009), 115001.
[5] D. Alveringh, R.A. Brookhuis, R.J. Wiegerink, G.J.M. Krijnen, A Large Range Multi-axis Capacitive force/torque Sensor Realized in a Single SOI Wafer, IEEE MEMS, San Francisco, CA, 2014, pp. 680–683.
[6] Y. Hata, Y. Suzuki, M. Muroyama, T. Nakayama, Y. Nonomura, R. Chand, H. Hirano, Y. Omura, M. Fujiyoshi, S. Tanaka, Integrated 3-axis tactile sensor using quad-seesaw-electrodestructure on platform LSI with through silicon vias, Sens. Actuators A Phys. 273 (2018) 30–41.
[7] S. Asano, M. Muroyama, T. Bartley, T. Kojima, T. Nakayama, U. Yamaguchi, H. Yamada, Y. Nonomura, Y. Hata, H. Funabashi, S. Tanaka, Surface-mountable capacitive tactile sensors with flipped CMOS-diaphragm on a flexible and stretchable bus line, Sens. Actuators A Phys. 240 (2016) 167–176.
[8] Y.-C. Liu, C.-M. Sun, L.-Y. Lin, M.-H. Tsai, W. Fang, Development of a CMOS-based capacitive tactile sensor with adjustable sensing range and sensitivity using polymer fill-in, J. Microelectromechanical Syst. 20 (2011) 119–127.
[9] W.-C. Lai, W. Fang, Novel Two-stage CMOS-MEMS Capacitive-type Tactile-sensor With ER-fluid Fill-in for Sensitivity and Sensing Range Enhancement, Transducers, Anchorage, Alaska, 2015, pp. 1175–1178.
[10] S.-Y. Tu, W.-C. Lai, W. Fang, Vertical Integration of Capacitive and Piezo-resistive Sensing Units to Enlarge the Sensing Range of CMOS-MEMS Tactile Sensor, IEEE MEMS, Las Vegas, NV, 2017, pp. 1048–1051.
[11] E.-S. Hwang, J.-H. Seo, Y.-J. Kim, A polymer-based flexible tactile sensor for both normal and shear load detections and its application for robotics, J. Microelectromechanical Syst. 16 (2007) 556–563.
[12] D.V. Dao, S. Sugiyama, Fabrication and characterization of 4-DOF soft-contact tactile sensor and application to robot fingers, in: IEEE International Symposium on MicroNanoMechanical and Human Science, Nagoya, Japan, 2006, pp. 1–6.
[13] T.-V. Nguyen, B.-K. Nguyen, H. Takahashi, K. Matsumoto, I. Shimoyama, High-sensitivity triaxial tactile sensor with elastic microstructures pressing on piezoresistive cantilevers, Sens. Actuators A Phys. 215 (2014) 167–175.
[14] H. Takahashi, A. Nakaia, N. Thanh-Vinh, K. Matsumoto, I. Shimoyama, A triaxial tactile sensor without crosstalk using pairs of piezoresistive beams with sidewall doping, Sens. Actuators A Phys. 199 (2013) 43–48.
[15] C.-Y. Huang, W.-L. Sung, W. Fang, Develop and Implement a Novel Tactile Sensor Array With Stretchable and Flexible Grid-like Spring, IEEE Sensors, Glasgow, UK, 2017, pp. 1–3.
[16] C.-C. Wen, W. Fang, Tuning the sensing range and sensitivity of three axes tactile sensors using the polymer composite membrane, Sens. Actuators A Phys. 145 (2008) 14–22.
[17] M. Ádám, T. Mohácsy, P. Jónás, C. Dücsö, E. Vázsonyi, I. Bársony, CMOS integrated tactile sensor array by porous Si bulk micromachining, Sens. Actuators A Phys. 142 (2008) 192–195.
[18] J.-H. Lee, S.-K. Yeh, W. Fang, Monolithic/vertical Integration of Piezo-resistive Tactile Sensor and Inductive Proximity Sensor Using CMOS-MEMS Technology, IEEE MEMS, Seoul, Korea, 2019, pp. 826–829.
[19] G. Vásárhelyi, M. Ádám, É. Vázsonyi, Z. Vízváry, A. Kis, I. Bársony, C. Dücsö, Characterization of an integrable single-crystalline 3-D tactile sensor, IEEE Sens. J. 6 (2006) 928–934.
[20] T. Lomas, A. Tuantranont, A. Wisitsoraat, Polysilicon Piezoresistive Tactile Sensor Array Fabricated by PolyMUMPS Process, IEEE Sensors, Daegu, Korea, 2006, pp. 1313–1316.
[21] J.-H. Kim, W.-C. Choi, H.-J. Kwon, D.-I. Kang, Development of Tactile Sensor With Functions of Contact Force and Thermal Sensing for Attachment to Intelligent Robot Finger Tip, IEEE Sensors, Daegu, Korea, 2006, pp. 1468–1472.
[22] C.-L. Cheng, M.-H. Tsai, W. Fang, Determining the thermal expansion coefficient of thin films for a CMOS MEMS process using test cantilevers, J. Micromechanics Microengineering 25 (2015), 025014.

[23] S. Wattanasarn, K. Noda, K. Matsumoto, I. Shimoyama, 3D Flexible Tactile Sensor Using Electromagnetic Induction Coils, IEEE MEMS, Paris, France, 2012, pp. 488–491.

[24] H.-C. Chang, W.-L. Sung, H.-S. Hsieh, J.-H. Wen, C.-C. Fu, S.-C. Liao, C.-H. Lai, W.-C. Lai, C.-H. Chang, C.-P. Chang, C.-H. Chen, W. Fang, Magnetostrictive Type Tactile Sensor Based on Metal Embedded Polymer Architecture, IEEE MEMS, San Francisco, CA, 2014, pp. 1189–1192.

[25] H. Wang, J. Kow, N. Raske, G.D. Boer, M. Ghajari, R. Hewson, A. Alazmani, P. Culmer, Robust and high-performance soft inductive tactile sensors based on the Eddy-current effect, Sens. Actuators A Phys. 271 (2018) 44–52.

[26] S.-K. Yeh, H.-C. Chang, W. Fang, Development of CMOS MEMS inductive type tactile sensor with the integration of chrome steel ball force interface, J. Micromechanics Microengineering 28 (2018), 044005.

[27] S.-K. Yeh, H.-C. Chang, C.-E. Lu, W. Fang, A CMOS-MEMS Electromagnetic-type Tactile Sensor With Polymer-filler and Chrome-steel Ball Sensing Interface, IEEE Sensors, New Delhi, India, 2018, pp. 1–4.

[28] S.-K. Yeh, W. Fang, Inductive micro tri-axial tactile sensor using a CMOS chip with a coil array, IEEE Electron Device Lett. 40 (2019) 620–623.

[29] S.-K. Yeh, W. Fang, Flip-chip Integration of Inductive CMOS Tactile Sensor With Si Cavity for polymer-filler/metal-ball Sensing Interface, IEEE MEMS, Seoul, Korea, 2019, pp. 833–836.

[30] T.K. Kim, J.K. Kim, O.C. Jeong, Measurement of nonlinear mechanical properties of PDMS elastomer, Microelectron. Eng. 88 (2011) 1982–1985.

[31] I.D. Johnston, D.K. McCluskey, C.K.L. Tan, M.C. Tracey, Mechanical characterization of bulk Sylgard 184 for microfluidics and microengineering, J. Micromechanics Microengineering 24 (2014), 035017.

[32] S.-H. Yoon, V. Reyes-Ortiz, K.-H. Kim, Y.H. Seo, M.R.K. Mofrad, Analysis of circular PDMS microballoons with ultralarge deflection for MEMS design, J. Microelectromechanical Syst. 19 (2010) 854–864.

[33] D.C. Larbalestier, H.W. King, Austenitic stainless steels at cryogenic temperatures- Structural stability and magnetic properties, Cryogenics 13 (1973) 160–168.

[34] P. Oxley, J. Goodell, R. Molt, Magnetic properties of stainless steels at room and cryogenic temperatures, J. Magn. Magn. Mater. 321 (2009) 2107–2114.

[35] Engineering ToolBox, Permeability, Accessed: July 16, 2019. Available:, 2016 https://www.engineeringtoolbox.com/permeability-d_1923.html.

[36] A. Belhadj, P. Baudouin, F. Breaban, A. Deffontaine, M. Dewulf, Y. Houbaert, Effect of laser cutting on microstructure and on magnetic properties of grain non-oriented electrical steels, J. Magn. Magn. Mater. 256 (2003) 20–31.

Biographies

Sheng-Kai Yeh was born in Taichung, Taiwan. In 2016, he received his B.S. degree from the Department of Power Mechanical Engineering, National Tsing Hua University, Taiwan. In 2017, he received his M.S. degree from the Department of Power Mechanical Engineering, National Tsing Hua University, Taiwan. He is currently a Ph.D. student in the Department of Power Mechanical Engineering, National Tsing Hua University, Taiwan. His research interests include design and implementation of the micro tactile sensor, contact interface design/integration of the micro tactile sensor, and the implementation of CMOS-MEMS sensors.

Jiunn-Horng Lee was born in Kaohsiung, Taiwan. He received his M.S. degrees from the Department of Mechanical Engineering, National Cheng-Kung University, Taiwan, in 1991. He received his Ph.D. degree from the Institute of NanoEngineering and MicroSystems, National Tsing Hua University, Taiwan, in 2010. He joined National Center for High-performance Computing, National Applied Research Laboratories, Taiwan, in 1991, where he is now an associate researcher. His research interests include computer-aided analysis of MEMS, solid mechanics and high-performance computing.

Weileun Fang was born in Taipei, Taiwan. He received his Ph.D. degree from Carnegie Mellon University in 1995. His doctoral research focused on the determining of the mechanical properties of thin films using micromachined structures. In 1995, he worked as a postdoctoral research at Synchrotron Radiation Research Center, Taiwan. He joined the Power Mechanical Engineering Department at the National Tsing Hua University (Taiwan) in 1996, where he is now a Chair Professor as well as a faculty of NEMS Institute. In 1999, he was with Prof. Y.-C. Tai at California Inst. Tech. as a visiting associate. He became the IEEE Fellow in 2015 to recognize his contribution in MEMS area. His research interests include MEMS with emphasis on micro fabrication/packaging technologies, CMOS MEMS, CNT MEMS, micro optical systems, micro sensors and actuators, and characterization of thin film mechanical properties. He is now the Chief Editor of JMM, the Associate Editor of IEEE Sensors Journal, and the Board Member of IEEE Transactions on Device and Materials Reliability. He served as the member of ISC (International steering committee) of Transducers in 2009–2017, and the ISC chair in 2017-2019. He also served as the General Chair of Transducers Conference in 2017. He was the TPC of IEEE MEMS and EPC of Transducers for many years, and the Program Chair of IEEE Sensors Conference in 2012. He served as the Chief Delegate of Taiwan for the World Micromachine Summit (MMS) in 2008–2012, and the General Chair of MMS in 2012. Prof. Fang has close collaboration with MEMS industries and is now the VP of MEMS and Sensors Committee of SEMI Taiwan.